

# Accepted Manuscript

Title: Composites of Ionic Liquid and Amine-modified SAPO 34 Improve CO<sub>2</sub> Separation of CO<sub>2</sub>-selective Polymer Membranes

Authors: Leiqing Hu, Jun Cheng, Yannan Li, Jianzhong Liu, Li Zhang, Junhu Zhou, Kefa Cen



PII: S0169-4332(17)30696-7

DOI: <http://dx.doi.org/doi:10.1016/j.apsusc.2017.03.045>

Reference: APSUSC 35421

To appear in: APSUSC

Received date: 25-11-2016

Revised date: 25-2-2017

Accepted date: 4-3-2017

Please cite this article as: Leiqing Hu, Jun Cheng, Yannan Li, Jianzhong Liu, Li Zhang, Junhu Zhou, Kefa Cen, Composites of Ionic Liquid and Amine-modified SAPO 34 Improve CO<sub>2</sub> Separation of CO<sub>2</sub>-selective Polymer Membranes, Applied Surface Science <http://dx.doi.org/10.1016/j.apsusc.2017.03.045>

This is a PDF file of an unedited manuscript that has been accepted for publication. As a service to our customers we are providing this early version of the manuscript. The manuscript will undergo copyediting, typesetting, and review of the resulting proof before it is published in its final form. Please note that during the production process errors may be discovered which could affect the content, and all legal disclaimers that apply to the journal pertain.

# Composites of Ionic Liquid and Amine-modified SAPO 34 Improve CO<sub>2</sub> Separation of CO<sub>2</sub>-selective Polymer Membranes

Leiqing Hu<sup>a</sup>, Jun Cheng<sup>a\*</sup>, Yannan Li<sup>a</sup>, Jianzhong Liu<sup>a</sup>, Li Zhang<sup>b</sup>, Junhu Zhou<sup>a</sup>, Kefa Cen<sup>a</sup>

<sup>a</sup>*State Key Laboratory of Clean Energy Utilization, Zhejiang University, Hangzhou 310027, China*

<sup>b</sup>*Shandong Botong New Energy Company, Jining 272000, China*

\* Corresponding author: Prof. Dr. Jun Cheng, State Key Laboratory of Clean Energy Utilization, Zhejiang University, Hangzhou 310027, China. Tel.: +86 571 87952889; fax: +86 571 87951616. E-mail: juncheng@zju.edu.cn

## Highlights

- > SAPO 34 was modified with amine groups to improve CO<sub>2</sub>/H<sub>2</sub> selectivity of MMM.
- > IL was loaded on modified SAPO 34 to enhance cohesion between SAPO 34 and polymer.
- > MMM surface became smooth after SAPO 34 was modified with NH<sub>2</sub> groups and IL.
- > Both CO<sub>2</sub> permeability and selectivity of MMM increased after the modification.
- > CO<sub>2</sub>/H<sub>2</sub> selectivity of MMM with IL/SAPO 34-NH<sub>2</sub> reached up to 22.1 at 20 °C.

## Abstract

Mixed matrix membranes with ionic liquids and molecular sieve particles had high CO<sub>2</sub> permeabilities, but CO<sub>2</sub> separation from small gas molecules such as H<sub>2</sub> was dissatisfied because of bad interfacial interaction between ionic liquid and molecular sieve particles. To solve that, amine groups were introduced to modify surface of

molecular sieve particles before loading with ionic liquid. SAPO 34 was adopted as the original filler, and four mixed matrix membranes with different fillers were prepared on the outer surface of ceramic hollow fibers. Both surface voids and hard agglomerations disappeared, and the surface became smooth after SAPO 34 was modified by amine groups and ionic liquid [P<sub>66614</sub>][2-Op]. Mixed matrix membranes with composites of amine-modified SAPO 34 and ionic liquid exhibited excellent CO<sub>2</sub> permeability (408.9 Barrers) and CO<sub>2</sub>/H<sub>2</sub> selectivity (22.1).

Abbreviation: P, permeability; D, diffusivity; S, solubility. PDMS, polydimethylsiloxane; PIMs, polymers of intrinsic microporosity; MOFs, metal organic frameworks; MMM, mixed matrix membrane; IL, ionic liquid; APTES, (3-aminopropyl)triethoxysilane; DBD, ditin butyl dilaurate; FTIR, fourier transform infrared. TGA, thermogravimetric analysis. SEM, scanning electron microscope. AFM, atomic force microscope.

**Keywords:** CO<sub>2</sub> separation, mixed matrix membranes, amine-modified SAPO 34, ionic liquid, hollow fiber.

## 1. Introduction

CO<sub>2</sub> separation using polymer membranes has drawn much attention because of its low cost, easy operation, and low energy demands [1]. These technologies include CO<sub>2</sub>/H<sub>2</sub> separation for hydrogen purification in IGCC processes, CO<sub>2</sub>/CH<sub>4</sub> separation for natural gas, and biogas purification [2, 3]. CO<sub>2</sub>-selective membranes for gas separation exhibit several specific properties. In these membranes, due to its good condensability and higher solubility in dense polymer matrix, CO<sub>2</sub> can obtain higher permeability than small gas molecules, such as H<sub>2</sub> [4]. This property depends on whether molecular transport through these membranes is governed by the

solution–diffusion model. The permeability  $P$  under the solution–diffusion model can be expressed as  $P = S \times D$ , where  $S$  and  $D$  represent solubility (solution coefficient,  $S$  determined by gas condensability) and diffusivity (diffusion coefficient), respectively [5]. With its higher condensability,  $\text{CO}_2$  exhibits higher solubility than that of other gases, such as  $\text{H}_2$  and  $\text{CH}_4$ .  $D$  depends on both gas molecular diameter and size-sieving ability of the polymer chains [6]. Therefore, small gas molecules exhibit high diffusion coefficients. The permeability of  $\text{CO}_2$  can be increased by enhancing the solution function and weakening the diffusion function. Moreover, the increase in  $S_{\text{CO}_2}$  does not mean an increase in the solubility of other gases; as such,  $\text{CO}_2$ -selective membranes can overcome the trade-off limitation between  $\text{CO}_2$  permeability and selectivity that occurs in a conventional polymer membrane [7].  $\text{CO}_2$ -selective membranes are prepared using common polymer materials, namely,  $\text{CO}_2$ -philic polymers, including polydimethylsiloxane (PDMS), PEO-based polymers, and several polymers of intrinsic microporosity (PIMs) [8]. However, the permeation and separation performance of these membranes does not reach the required level to be economically competitive with other existing separation technologies [7]. To improve the performance of these membranes, scholars have proposed several approaches, including blending porous materials (such as carbon nanotubes, zeolites, molecular sieves, and MOFs) into membrane materials to obtain mixed-matrix membranes (MMMs) [8]. Most of MMMs showed improved mechanical and chemical resistances [8]. Meanwhile, some of these membranes exhibit excellent transport property of the porous particles [9-11]. However, because of the poor compatibility between those particles and  $\text{CO}_2$ -philic polymers,

voids are produced at the interface of the two phases [12]. In this regard, ionic liquids (ILs) are introduced to modify the surface of the porous particles and enhance the adhesion between the particles and the polymers. Hudiono et al. [13-15] investigated the effects of blending ILs and zeolites into poly(IL) and found that the interaction among the three components was promoted. Hao et al. introduced ZIF-8 nanoparticles into poly(IL)/IL membranes to increase the CO<sub>2</sub> permeability [16]. Ryohei Shindo et al. [17] added IL and ZSM-5 into a polyimide solution and found that CO<sub>2</sub>/H<sub>2</sub> selectivity and CO<sub>2</sub>/CH<sub>4</sub> selectivity were improved but CO<sub>2</sub> permeability was decreased. However, most membranes in these studies were prepared by separately blending ILs and porous particles into polymer solutions. As such, the advantages of blending porous particles were lost. In two other studies, MOFs were loaded with ILs before being added into the polymer solutions, and the effects of blending composites of ILs and MOFs were determined [12, 18]. However, the CO<sub>2</sub>/H<sub>2</sub> selectivity of the membranes was either too low or difficult to determine. ILs and porous particles were freely distributed and exhibited minimal interaction with each other. As a result, these porous particles enhanced the size-sieving ability of the membrane, thereby enlarging the gap of diffusivity between CO<sub>2</sub> and H<sub>2</sub>. Although the ILs were loaded into the inner pores of MOFs or covered onto the outer surface of MOFs, CO<sub>2</sub>/H<sub>2</sub> selectivities of their membranes were still low. This feature could be due to the fact that ILs cannot completely cover the surface of porous particles and uncovered pores provided inner channels for H<sub>2</sub> transport.

In this study, SAPO 34 was adopted as porous filler, the structure of SAPO 34 was

shown in Fig. 1 (a). The pore diameter of SAPO 34 is 0.38 nm, which is larger than the kinetic diameters of CO<sub>2</sub> (0.33 nm) and equal to the kinetic diameters of CH<sub>4</sub> (0.38 nm) [9]. Therefore, SAPO 34 is considered to be an useful filler for CO<sub>2</sub>/CH<sub>4</sub> separation [19]. Meanwhile, several MMMs with SAPO 34 have showed improved CO<sub>2</sub> separation performance from CH<sub>4</sub> [19-21]. Amine groups were introduced onto the surface of SAPO 34 particles through the chemical reaction between (3-aminopropyl)triethoxysilane (APTES) and hydroxyl. Amine groups on the surface of SAPO 34-NH<sub>2</sub> (which stands for SAPO 34 that had been modified with NH<sub>2</sub> group) could inhibit H<sub>2</sub> molecules from entering through the inner channels of the particles, consequently enhancing CO<sub>2</sub> selectivity. One IL was then loaded onto the particles to enhance the cohesion between SAPO 34 and CO<sub>2</sub>-philic polymer. The IL [P<sub>66614</sub>][2-Op] was adopted in this study and proven to exhibit high CO<sub>2</sub> capacity (up to 1.60 mol CO<sub>2</sub> per mol IL) and satisfactory CO<sub>2</sub> transport property [22, 23]. The combined action of amine groups (NH<sub>2</sub> groups) and IL could minimize the loss of CO<sub>2</sub> selectivity and improve the CO<sub>2</sub>/H<sub>2</sub> selectivity. Two different amounts of ILs were blended with SAPO 34-NH<sub>2</sub> to determine the effects of blending IL/SAPO 34-NH<sub>2</sub> composites into the CO<sub>2</sub>-philic polymer when the surface of SAPO 34-NH<sub>2</sub> is being fully or partially covered by IL. One of the prepared IL/SAPO 34-NH<sub>2</sub> composite with high content of IL was dense liquid, and SAPO 34-NH<sub>2</sub> was dispersed in IL. Therefore, the complete covering of IL on the surface of SAPO 34-NH<sub>2</sub> was guaranteed. The other prepared IL/SAPO 34-NH<sub>2</sub> composite with lower content of IL was off-white solid, indicating that the IL did not fully cover the surface of SAPO 34-NH<sub>2</sub>. Furthermore, MMMs in

other studies exhibited a flat form and CO<sub>2</sub> permeation rates that were either too low or difficult to determine. In the present study, ceramic hollow fiber-supported MMMs were fabricated. A ceramic hollow fiber-supported membrane structure has all the advantages of a hollow fiber membrane (such as easy assembling and large surface area per unit volume of membrane material) and maintained the good mechanical and thermal stabilities of ceramics [24]. In addition, Pebax/PEGDME blend was adopted as CO<sub>2</sub>-philic polymer. Pebax/PEGDME blend have showed high CO<sub>2</sub> permeability, CO<sub>2</sub>/H<sub>2</sub> selectivity and CO<sub>2</sub>/CH<sub>4</sub> selectivity [25].

## 2. Experimental

### 2.1. Materials

The IL [P<sub>66614</sub>][2-Op] was purchased from the Department of Chemistry, ZJU-NHU United R&D Centre at Zhejiang University, China. SAPO 34 was bought from the Catalyst Plant of Nankai University. The kind of Pebax used in this study is Pebax® MH 1657, which was provided by Arkema Company. Poly(ethylene glycol) dimethyl ether (PEGDME) (average M.W. \_500) and (3-Aminopropyl)triethoxysilane was obtained from Sigma-Aldrich Company. Ditin butyl dilaurate (DBD, as catalyst) was obtained from Aladdin Inc. and used as received. Asymmetric  $\alpha$ -Al<sub>2</sub>O<sub>3</sub> ceramic hollow fibers were provided by the State Key Laboratory of Chemical Engineering at Zhejiang University, China. Torr Seal was purchased from Shanghai Passion Auto & Tec Company.

## 2.2. Preparation of IL/SAPO 34 (1:4), IL/SAPO 34-NH<sub>2</sub> (1:4), and IL/SAPO 34-NH<sub>2</sub> (1:2) composites

Three composites were prepared, namely, IL/SAPO 34 (1:4), IL/SAPO 34-NH<sub>2</sub> (1:4), IL/SAPO 34-NH<sub>2</sub> (1:2), where 1:4 and 1:2 indicate the weight ratios of IL to SAPO 34 (or IL to SAPO 34-NH<sub>2</sub>). To produce the IL/SAPO 34 (1:4) composite, 2 g of SAPO 34 and 0.5 g of IL were simultaneously added into 30 g of ethanol solution. The solution was stirred and refluxed at 353 K for 3 h, and then dried in a blast oven at 353 K until the ethanol was volatilized. The dried solid mixture is the IL/SAPO 34 (1:4) composite.

The preparation of IL/SAPO 34-NH<sub>2</sub> (1:4) and IL/SAPO 34-NH<sub>2</sub> (1:2) composites included two steps, as shown in Fig. 1 (b). The first step was the amino modification on the surface of SAPO 34. Firstly, 2 g of SAPO 34 were added into 30 g of toluene, and then dissolved under magnetic stirring for about 10 min. After SAPO 34 was completely dissolved, 0.2 g of APTES and 0.1 g of DBD were added into the solution. The solution was stirred and heated to 110 °C under N<sub>2</sub> atmosphere. The reaction for amino modification on SAPO 34 was performed for 3 h. After that, the solution was dried at 120 °C to remove toluene, and modified SAPO 34 particles were obtained. The second step was the combination of SAPO 34 and IL. Both modified SAPO 34 and IL were added into 30 g of ethanol. The weight ratios of IL/SAPO 34 were 1/4 and 1/2, respectively. The mixture was stirred and refluxed at 353 K for 3 h, and then dried in a blast oven at 353 K until the ethanol was volatilized. Finally, IL/SAPO 34-NH<sub>2</sub> (1:4) and IL/SAPO 34-NH<sub>2</sub> (1:2) composites were prepared. The

IL/SAPO 34-NH<sub>2</sub> (1:4) composite is solid, while the IL/SAPO 34-NH<sub>2</sub> (1:2) composite is thick.

### **2.3. Preparation of MMM coating solutions**

The Pebax/PEGDME solution was prepared using a method described in a previous study [23]. Approximately 1.5 g of Pebax MH 1657 pellets were dissolved in 28.5 g of ethanol/water solvent (70/30, weight ratio). The polymer solution was stirred under reflux at 80 °C for more than 3 h until complete dissolution. After cooling to room temperature, 1.5 g of PEGDME was added into the solution, and then stirred for about 1 h at room temperature. The obtained homogeneous solution was filtered through a stainless steel filter with a pore size of 32 µm and was designated as the Pebax/PEGDME coating solution. One of four fillers (SAPO 34, IL/SAPO 34, and two IL/SAPO 34-NH<sub>2</sub> composites) was then added to the solution to prepare coating solutions. The mass ratio of samples and Pebax in coating solutions was 1/10. The solution was stirred for 0.5 h at room temperature, placed in a microwave bath, and vibrated for 15 min to ensure that the sample was evenly distributed in the solution.

### **2.4. Preparation of MMMs**

Four MMMs were fabricated, namely, MMM with SAPO 34, MMM with IL/SAPO 34 (1:4), MMM with IL/SAPO 34-NH<sub>2</sub> (1:4), and MMM with IL/SAPO 34-NH<sub>2</sub> (1:2). In this study, membranes were prepared on ceramic hollow fibers through a two-time dip coating process. At first, one end of the ceramic hollow fiber

was inserted and attached to a stainless steel capillary, while the other end was sealed with Torr Seal. After being pre-wetted by deionized water for about 10 s, the ceramic hollow fiber was immersed into the coating solution for 5 s. Then, the hollow fiber was rotated at 100r/min for 15 min and dried at room temperature for another 3 h. The dried hollow fiber was then immersed again into the coating solution for 5 s, rotated at 100r/min for 15 min, and dried again at room temperature for more than 12 h. Finally, the selective layer was then formed on the surface of the ceramic hollow fiber.

## 2.5. Membrane characterization

To obtain the Fourier transform infrared (FTIR) spectra of SAPO 34 and those after being modified with amine groups and IL, a Nicolet 5700 FTIR spectrometer with a scan range of  $4000\text{ cm}^{-1}$  to  $400\text{ cm}^{-1}$  and a resolution of  $0.09\text{ cm}^{-1}$  was used.

The thermal stability of IL, SAPO 34, and the three other SAPO 34 samples modified with APTES and IL was detected by thermo-gravimetric analysis (TGA, TA-Q500, USA). The temperature inside the furnace was increased from  $30\text{ }^{\circ}\text{C}$  to  $800\text{ }^{\circ}\text{C}$  at a rate of  $10\text{ }^{\circ}\text{C}/\text{min}$  under air atmosphere.

The surface changes in MMMs after surface modifications with SAPO 34 particles, as well as the junction effectiveness between the different selective layers and ceramic hollow fiber supports, were analyzed using a Hitachi SU-70 field-emission scanning electron microscope (FESEM, FEG650, FEI, Holland) operated at  $3\text{ kV}$ . Prior to the analysis, MMMs were cryogenically fractured in liquid nitrogen and then sputtered with a thin layer of gold.

The surface morphology of the four MMMs was also observed by a VEECO Multi-Mode atomic force microscopy (AFM). AFM was conducted at room temperature with dried hollow fiber-supported MMMs.

## 2.5. Gas permeation test

Four types of MMMs were successfully fabricated. Each membrane consisted of three samples fabricated under similar conditions. Gas permeation measurements were also conducted at different operating temperatures (10–50 °C) and under 1 bar (relative pressure) to evaluate CO<sub>2</sub> permeation and separation performance of MMMs. The apparatus for the measurement of gas permeance was shown in fig. 2. The operating temperature was measured with a thermometer and controlled in a constant low-temperature bath (Hangzhou David Science Instrument Co., GDC1015, China). The feed pressure was measured with digital pressure gauges (Spectris, DPG409-150A, China). Pure CO<sub>2</sub>, pure H<sub>2</sub>, and pure CH<sub>4</sub> were adopted as feed gases. Ar was used as the sweep gas at atmospheric pressure and room temperature. The flow rates of the individual gases were controlled using mass flow controllers (Seven Star, CS200C, China). The composition of the permeate gas was analyzed by gas chromatography (Agilent, 7820A, USA). Gas permeability and selectivity were calculated using Equations 1–2 [5, 26]:

$$P = Q \bullet L / (S_m \Delta p) \quad (1)$$

$$\alpha_{A/B} = P_A / P_B \quad (2)$$

where  $P$  is the gas permeability coefficient (Barrer, 1 Barrer = 1 × 10<sup>-10</sup>

$\text{cm}^3(\text{STP}) \cdot \text{cm}/\text{cm}^2 \cdot \text{s} \cdot \text{cm Hg}$ ,  $L$  is the thickness of the selective layer,  $Q$  represents the gas flow rate,  $S_m$  is the effective permeation area of the composite membrane, and  $\Delta p$  is the pressure difference across the membrane. Gas selectivity  $\alpha_{A/B}$  is the ratio of  $P_A$  to  $P_B$ .

### 3. Results and discussion

#### 3.1. Membrane characterization

Fig. 3 shows FTIR spectra of IL [P<sub>66614</sub>][2-Op], SAPO 34, two IL/SAPO 34-NH<sub>2</sub> composites, and IL/SAPO 34 composite. For SAPO 34, the peak at 1632 cm<sup>-1</sup> is attributed to physically absorbed water, which has been tested by TGA [27]. Meanwhile, the band around 3450 cm<sup>-1</sup> was related to structural O–H for the Si(OH)Al bridging hydroxyl group [28]. Moreover, the peak at 1102 cm<sup>-1</sup> represents the P–O–P stretching band [27]. For IL spectrum, the characteristic peaks at 2852 and 2922 cm<sup>-1</sup> represent the stretching vibrations of C–H and C–CH<sub>3</sub>, respectively [23]. All peaks in the spectra of the two IL/SAPO 34-NH<sub>2</sub> composites show proportional intensity with the weight percentage of IL and SAPO 34. Because SAPO 34 was not modified with APTES, the peak for the O–H band of the IL/SAPO 34 composite was relatively stronger than those of the two IL/SAPO 34-NH<sub>2</sub> composites.

TGA on thermal stability of IL, SAPO 34 particles, IL/SAPO 34 (1:4), IL/SAPO 34-NH<sub>2</sub> (1:4), and IL/SAPO 34-NH<sub>2</sub> (1:2) composites is shown in Fig. 4. All samples were pretreated at 80 °C for 5 min to remove moisture and remaining ethanol. Then, the temperature was lowered to 50 °C, and thermal stability was estimated within the

range of 50–800 °C. For IL, the weight loss starts at about 180 °C and is completed at 380 °C. For SAPO 34, a slight weight loss of 0.5% is attributed to the residual moisture in the pores [29]. The weight losses of IL/SAPO 34 (1:4), IL/SAPO 34-NH<sub>2</sub> (1:4), and IL/SAPO 34-NH<sub>2</sub> (1:2) are 22.5%, 26.7%, and 42.1%, respectively. The weight losses are basically consistent with designed IL loadings, regardless of whether or not SAPO 34 was modified with APTES. Furthermore, for both IL/SAPO 34-NH<sub>2</sub> samples, the weight loss starts at about 100 °C because of the pyrolysis of APTES and residual DBD.

SEM analysis was conducted to observe the surface changes of MMMs after surface modifications of SAPO 34 particles. The typical surface and cross-sectional SEM images are presented in Fig. 5. From those surface images, no defect in any sample can be seen. Moreover, good mix between polymer and fillers is present. Also, the three cross-sectional images show that all CO<sub>2</sub>-philic selective layers closely adhered to ceramic hollow fibers, while the three phases were homogeneous in the membranes. However, obvious differences in surface morphology among the four membranes can be observed from surface images. Comparing Fig. 5 (a) with three other surface images, we found that after surface modification of SAPO 34, less particles were distributed on the surface and the surface became smoother. This can be attributed to the decreasing amount of SAPO 34, as well as the good compatibility between these particles and polymers, after surface modification [12]. In Fig. 5 (c), several large particles existed on the surface of the MMM with IL/SAPO 34 (1:4). Because the IL/SAPO 34 (1:4) composite had sticky solid particles and was not

modified by the NH<sub>2</sub> group, the surface of SAPO 34 particles had been covered only with IL ions. As a result, IL ions on the surface of SAPO 34 attract each other under the action of intermolecular hydrogen bonds [23]. Therefore, evenly distributing those particles into the polymer is hard, whereas producing small agglomerations is easy. Furthermore, an increase in the amount of added IL led to a corresponding decrease in the amount of SAPO 34-NH<sub>2</sub> particles. As such, the amount of particles distributed on the surface of Fig.5 (g) is less than that distributed on surface of Fig 5 (e). Moreover, the thickness of each selective layer was measured based on 10 cross-sectional images. All thicknesses were measured at 8 μm with errors of less than 6%.

AFM was also conducted to analyze surface roughness and phase separation of four MMMs. Ten 10 μm × 10 μm samples for each MMM were tested and typical samples are shown in Figs. 6 and 7. As seen in Fig. 6 (a), many small voids were observed. This is because of the poor compatibility between SAPO 34 and Pebax/PEGDME blends [12, 13]. The large amount of isolated SAPO 34 particles distributed on the surface causes greater roughness. As such, R<sub>ms</sub> and R<sub>a</sub> (representing the root-mean-square deviation of height and average deviation of height, respectively), evaluated at 37.5 and 30.1, are larger than those for the three other MMMs, as shown in Table 1. Furthermore, as shown in Fig. 7 (a) and (b), the phase separation is most obvious in the MMM with SAPO 34, but is rather not obvious in the MMM with IL/SAPO 34 (1:4). The adhesion between SAPO 34 particles and polymer chains was enhanced by IL existing on the surface of SAPO 34 particles [14]. Large hard bulks also appeared at the phase image of the MMM with IL/SAPO 34

(1:4). In addition, because the amount of SAPO 34-NH<sub>2</sub> particles decreases, the hard phase in the MMM with IL/SAPO 34-NH<sub>2</sub> (1:2) was less than that in IL/SAPO 34-NH<sub>2</sub> (1:4) MMM.

### **3.2. Gas permeation and separation performance**

Four MMMs were fabricated: blending SAPO 34, blending IL/SAPO 34 (1:4), blending IL/SAPO 34-NH<sub>2</sub> (1:4), and blending IL/SAPO 34-NH<sub>2</sub> (1:2), as shown in Table 2. All the thicknesses of the four selective layers supported on the hollow fiber were estimated at 8 μm through SEM. The polymer in MMMs is the Pebax/PEGMDE composite. All data about permeation and separation performance of those membranes are listed in Table 2. Primarily, MMMs had a ~20% decrease of CO<sub>2</sub> permeability after SAPO 34 was blended into Pebax/PEGDME. This result is consistent with another study, and can be attributed to the increasing tortuosity for diffusion at low SAPO 34 loading, where the channel network is not yet mature [9]. Furthermore, SAPO 34 in Pebax/PEGDME membranes is not selective towards CO<sub>2</sub> or H<sub>2</sub>, and the kinetic diameters of H<sub>2</sub> (0.289 nm) and CO<sub>2</sub> (0.33 nm) are smaller than mean pore diameter of SAPO-34 [14]. Therefore, both CO<sub>2</sub> diffusivity and H<sub>2</sub> diffusivity could be improved. As a result, the diffusion selectivity of CO<sub>2</sub> against H<sub>2</sub> decreased, and in turn, CO<sub>2</sub>/H<sub>2</sub> selectivity decreased. While on CO<sub>2</sub>/H<sub>2</sub> solution selectivity, the effect of SAPO 34 is small. However, as the kinetic diameter of CH<sub>4</sub> is 0.38 nm, CH<sub>4</sub> gas molecules were, at certain extent, restricted from entering into the inner channels of SAPO 34 particles. This had a positive effect on CO<sub>2</sub>/CH<sub>4</sub>

selectivity. In addition, compared with Pebax/PEGDME/IL membrane, both MMMs with IL/SAPO 34-NH<sub>2</sub> composites have superior CO<sub>2</sub> permeability and CO<sub>2</sub>/H<sub>2</sub> selectivity. This is because NH<sub>2</sub> groups of amine-modified SAPO 34 can only react with CO<sub>2</sub>, while SAPO 34-NH<sub>2</sub> particles in membranes provide exclusive channels for CO<sub>2</sub> transport [7]. Comparing the four MMMs with each other, an improvement was found for CO<sub>2</sub> permeability after SAPO 34 was modified with APTES and IL. This result is consistent with other studies [13, 14]. The increase of CO<sub>2</sub> permeability could be attributed to two reasons. Firstly, because of the presence of the IL component, the free ion pairs tend to create and fill the volume between polymer chains, increasing the diffusivity, and in turn, permeability of gas molecules through the membrane (improving CO<sub>2</sub> permeability in polymerized room-temperature IL). Secondly, NH<sub>2</sub> units and IL on the surface of SAPO 34 could facilitate CO<sub>2</sub> transport [7]. Relative to the MMM with SAPO 34, CO<sub>2</sub>/H<sub>2</sub> and CO<sub>2</sub>/CH<sub>4</sub> selectivities decreased to 9.2 and 10.7 when only IL was loaded onto SAPO 34. However, they increased significantly after SAPO 34 was modified by both NH<sub>2</sub> groups and IL. Because the IL/SAPO 34 (1:4) composite had sticky solid particles and was not modified by the NH<sub>2</sub> group, the surface of the SAPO 34 particles had been covered only with IL ions, making small agglomerations easy to produce. Those agglomerations enlarge the gap between polymer chains, reducing CO<sub>2</sub> selectivity. However, when the surface of SAPO 34 was first modified with APTES, cohesion between IL/SAPO 34-NH<sub>2</sub> composites themselves were weakened because the interaction of APTES with IL was lower. This effect could decrease the possibility of

agglomeration and increase CO<sub>2</sub>/H<sub>2</sub> and CO<sub>2</sub>/CH<sub>4</sub> selectivities.

CO<sub>2</sub> permeation performance of the four MMMs is displayed in Fig. 8. After being modified with APTES and two different amounts of IL, all MMMs had improved CO<sub>2</sub> permeances, especially when the weight ratio of IL/SAPO 34-NH<sub>2</sub> was 1/2. For example, at 40 °C operating temperature, CO<sub>2</sub> permeances for the four MMMs with SAPO 34, IL/SAPO 34 (1:4), IL/SAPO 34-NH<sub>2</sub> (1:4), and IL/SAPO 34-NH<sub>2</sub> (1:2) were about 35 GPU, 65 GPU, 59 GPU, and 77 GPU, respectively. The improvement of CO<sub>2</sub> permeance of MMM by modification of APTES and IL is consistent in different operating temperatures. Furthermore, with an increase in the operating temperature, all CO<sub>2</sub> permeation rates increased linearly. Specifically, the CO<sub>2</sub> permeation rate of the MMM with IL/SAPO 34-NH<sub>2</sub> (1:2) increased from about 39 GPU at 10 °C to 94 GPU at 50 °C. This shows a growth rate of nearly 2.5 times. The same growth is also seen in the three other MMMs. Two main factors were considered in explaining the considerable increase in the permeation rate. First, the thermodynamic energy of CO<sub>2</sub> molecules improved with increasing temperature. Therefore, the mobility of CO<sub>2</sub> molecules increases, thereby enhancing the driving force for diffusion [11]. Moreover, the increase in the operating temperature led to more flexible polymer chains, thereby creating more free volume cavities for molecule transport [25]. Furthermore, the gaps in the CO<sub>2</sub> permeation rate between the MMM with SAPO 34 and the three other MMMs were enlarged with rising temperature. This was because the CO<sub>2</sub> absorption and desorption cycle of IL and NH<sub>2</sub> units were increased under high temperature, thereby increasing CO<sub>2</sub> transport

through the membrane [22].

The comparison of CO<sub>2</sub>/H<sub>2</sub> and CO<sub>2</sub>/CH<sub>4</sub> selectivities between the four MMMs, as well as effects of operating temperature, are presented in Fig. 9. For CO<sub>2</sub>/H<sub>2</sub> selectivity, surface modification with IL and APTES reduced H<sub>2</sub> molecules' advantage on the inner pore channels of SAPO 34, thereby improving CO<sub>2</sub>/H<sub>2</sub> selectivity. In addition, for MMMs with IL/SAPO 34-NH<sub>2</sub> (1:2) and IL/SAPO 34-NH<sub>2</sub> (1:4), pores of SAPO 34 particles with 0.38 nm diameter had a positive effect on CO<sub>2</sub>/CH<sub>4</sub> separation. The addition of IL and NH<sub>2</sub> units also enhanced CO<sub>2</sub> selectivity. The CO<sub>2</sub> selectivity of both MMMs with IL/SAPO 34-NH<sub>2</sub>, as well as the MMM with SAPO 34, decreased with an increase in the operating temperature. This is because of the low CO<sub>2</sub> solubility selectivity under higher temperature [11]. Furthermore, MMMs with IL/SAPO 34-NH<sub>2</sub> (1:2) obtained a CO<sub>2</sub>/H<sub>2</sub> selectivity of 28.5 at 10 °C, which was one of highest CO<sub>2</sub>/H<sub>2</sub> selectivities for PEO-based polymer membranes under similar conditions. Moreover, the lowest CO<sub>2</sub>/H<sub>2</sub> and CO<sub>2</sub>/CH<sub>4</sub> selectivities of MMMs with IL/SAPO 34 (1:4) was due to the agglomeration of IL/SAPO 34 particles. Meanwhile, CO<sub>2</sub>/H<sub>2</sub> and CO<sub>2</sub>/CH<sub>4</sub> selectivities increased when temperature increased from 10 °C to 30 °C. It rarely happened in membranes and was probably because that the increased temperature weaken the hydrogen bonds and interaction between IL and SAPO 34, thereby increasing the mobility of IL anions on SAPO 34 and then the CO<sub>2</sub> transport by IL [23].

The comparisons of CO<sub>2</sub> permeation and separation performance among different MMMs, as well as upper bound lines, are shown in Fig. 10 (a) and (b). For

CO<sub>2</sub>/H<sub>2</sub> separation, the performance of all four MMMs in this study either approached or surpassed the upper bound line proposed by Lin et al [5]. Compared with other reported membranes, both MMMs with IL/SAPO 34-NH<sub>2</sub> had relatively higher CO<sub>2</sub>/H<sub>2</sub> selectivities. Meanwhile, CO<sub>2</sub> permeabilities of both MMMs with IL/SAPO 34-NH<sub>2</sub> and MMM with IL/SAPO (1:4) were higher than those reported for MMMs with IL and molecular sieve particles together [12, 17, 18]. For CO<sub>2</sub>/CH<sub>4</sub> separation, the Robeson upper line was adopted and the temperature on data was regulated at 25 °C [30]. Although the operating temperature for those values in this study is 20 °C, the Robeson upper line still had reference function. Relative to MMMs in other studies and Robeson upper bound line, MMMs with IL/SAPO 34-NH<sub>2</sub> (1:2) and IL/SAPO 34-NH<sub>2</sub> (1:4) showed intermediate performance [12-18].

The performance of reported CO<sub>2</sub>-philic membranes in hollow fiber structure was also compared with the four MMMs in this research, as shown in Table 3 [23, 31-36]. Both MMMs with IL/SAPO 34-NH<sub>2</sub> (1:2) and IL/SAPO 34-NH<sub>2</sub> (1:4) had higher CO<sub>2</sub> permeation rates than most of the membranes. Moreover, among all hollow fiber CO<sub>2</sub>-philic membranes, the MMM with IL/SAPO 34-NH<sub>2</sub> (1:2) showed the highest CO<sub>2</sub>/H<sub>2</sub> selectivity, followed by the MMM with IL/SAPO 34-NH<sub>2</sub> (1:4). However, for CO<sub>2</sub>/CH<sub>4</sub> selectivity, all four MMMs showed modest performance.

#### 4. Conclusion

In summary, SAPO 34 particles modified with amine and IL were composited and then blended into a CO<sub>2</sub>-selective polymer, and ceramic hollow fiber-supported

MMMs were prepared. Surfaces of MMM with SAPO 34 became smoother and voids disappeared after SAPO 34 was modified with the NH<sub>2</sub> group and IL. After modification of SAPO 34 with IL, CO<sub>2</sub> permeability increased while CO<sub>2</sub>/H<sub>2</sub> and CO<sub>2</sub>/CH<sub>4</sub> selectivities decreased. However, both CO<sub>2</sub> permeability and CO<sub>2</sub> selectivity increased after SAPO 34 was modified with both the NH<sub>2</sub> group and IL. Meanwhile, MMM with IL/SAPO 34-NH<sub>2</sub> (1:2) exhibited excellent CO<sub>2</sub> permeability (408.9 Barrers) and CO<sub>2</sub>/H<sub>2</sub> selectivity (22.1) at 20 °C.

## Acknowledgements

This study was supported by the National Key Technology R&D Program-China (2015BAD21B01), National Natural Science Foundation-China (51676171), Zhejiang Provincial Natural Science Foundation-China (LR14E060002).

## References

- [1] Z. Kang, M. Xue, L. Fan, L. Huang, L. Guo, G. Wei, B. Chen, S. Qiu, Highly selective sieving of small gas molecules by using an ultra-microporous metal-organic framework membrane, *Energy Environ. Sci.*, 7 (2014) 4053-4060.
- [2] H.Q. Lin, Z.J. He, Z. Sun, J. Kniep, A. Ng, R.W. Baker, T.C. Merkel, CO<sub>2</sub>-selective membranes for hydrogen production and CO<sub>2</sub> capture - Part II: Techno-economic analysis, *J Membrane Sci.*, 493 (2015) 794-806.
- [3] J.E. Ramirez-Morales, E. Tapia-Venegas, N. Nemestothy, P. Bakonyi, K. Belafi-Bako, G. Ruiz-Filippi, Evaluation of two gas membrane modules for fermentative hydrogen separation, *International Journal Of Hydrogen Energy*, 38 (2013) 14042-14052.
- [4] M.K. Barillas, R.M. Enick, M. O'Brien, R. Perry, D.R. Luebke, B.D. Morreale, The CO<sub>2</sub> permeability and mixed gas CO<sub>2</sub>/H<sub>2</sub> selectivity of membranes composed of CO<sub>2</sub>-philic polymers, *J Membrane Sci.*, 372 (2011) 29-39.
- [5] H. Lin, E. Van Wagner, B.D. Freeman, L.G. Toy, R.P. Gupta, Plasticization-enhanced hydrogen purification using polymeric membranes, *Science*, 311 (2006) 639-642.
- [6] D. Zhao, J.Z. Ren, H. Li, X.X. Li, M.C. Deng, Gas separation properties of poly(amide-6-b-ethylene oxide)/amino modified multi-walled carbon nanotubes mixed matrix membranes, *Journal Of Membrane Science*, 467 (2014) 41-47.
- [7] Z.H. Qiao, Z. Wang, S.J. Yuan, J.X. Wang, S.C. Wang, Preparation and characterization of small molecular amine modified PVAm membranes for CO<sub>2</sub>/H<sub>2</sub> separation, *J Membrane Sci.*, 475 (2015) 290-302.

- [8] S. Wang, X. Li, H. Wu, Z. Tian, Q. Xin, G. He, D. Peng, S. Chen, Y. Yin, Z. Jiang, M.D. Guiver, Advances in high permeability polymer-based membrane materials for CO<sub>2</sub> separations, *Energy Environ. Sci.*, 9 (2016) 1863-1890.
- [9] D. Zhao, J. Ren, H. Li, K. Hua, M. Deng, Poly(amide-6-b-ethylene oxide)/SAPO-34 mixed matrix membrane for CO<sub>2</sub> separation, *Journal of Energy Chemistry*, 23 (2014) 227-234.
- [10] S.G. Lovineh, M. Asghari, G. Khanbabaei, CO<sub>2</sub> permeation through poly(amide-6-b-ethylene oxide)-nanosilica membranes, *Applied Surface Science*, 318 (2014) 176-179.
- [11] S.F. Wang, Y. Liu, S.X. Huang, H. Wu, Y.F. Li, Z.Z. Tian, Z.Y. Jiang, Pebax-PEG-MWCNT hybrid membranes with enhanced CO<sub>2</sub> capture properties, *J Membrane Sci*, 460 (2014) 62-70.
- [12] H. Li, L.H. Tuo, K. Yang, H.K. Jeong, Y. Dai, G.H. He, W. Zhao, Simultaneous enhancement of mechanical properties and CO<sub>2</sub> selectivity of ZIF-8 mixed matrix membranes: Interfacial toughening effect of ionic liquid, *J Membrane Sci*, 511 (2016) 130-142.
- [13] Y.C. Hudiono, T.K. Carlisle, J.E. Bara, Y.F. Zhang, D.L. Gin, R.D. Noble, A three-component mixed-matrix membrane with enhanced CO<sub>2</sub> separation properties based on zeolites and ionic liquid materials, *J Membrane Sci*, 350 (2010) 117-123.
- [14] Y.C. Hudiono, T.K. Carlisle, A.L. LaFrate, D.L. Gin, R.D. Noble, Novel mixed matrix membranes based on polymerizable room-temperature ionic liquids and SAPO-34 particles to improve CO<sub>2</sub> separation, *J Membrane Sci*, 370 (2011) 141-148.
- [15] Z.V. Singh, M.G. Cowan, W.M. McDanel, Y.W. Luo, R.F. Zhou, D.L. Gin, R.D. Noble, Determination and optimization of factors affecting CO<sub>2</sub>/CH<sub>4</sub> separation performance in poly(ionic liquid)-ionic liquid-zeolite mixed-matrix membranes, *Journal Of Membrane Science*, 509 (2016) 149-155.
- [16] L. Hao, P. Li, T.X. Yang, T.S. Chung, Room temperature ionic liquid/ZIF-8 mixed-matrix membranes for natural gas sweetening and post-combustion CO<sub>2</sub> capture, *Journal Of Membrane Science*, 436 (2013) 221-231.
- [17] R. Shindo, M. Kishida, H. Sawa, T. Kidesaki, S. Sato, S. Kanehashi, K. Nagai, Characterization and gas permeation properties of polyimide/ZSM-5 zeolite composite membranes containing ionic liquid, *Journal Of Membrane Science*, 454 (2014) 330-338.
- [18] Y.J. Ban, Z.J. Li, Y.S. Li, Y. Peng, H. Jin, W.M. Jiao, A. Guo, P. Wang, Q.Y. Yang, C.L. Zhong, W.S. Yang, Confinement of Ionic Liquids in Nanocages: Tailoring the Molecular Sieving Properties of ZIF-8 for Membrane-Based CO<sub>2</sub> Capture, *Angew Chem Int Edit*, 54 (2015) 15483-15487.
- [19] S.G. Li, J.L. Falconer, R.D. Noble, Improved SAPO-34 membranes for CO<sub>2</sub>/CH<sub>4</sub> separations, *Adv Mater*, 18 (2006) 2601-+.
- [20] S.G. Li, J.L. Falconer, R.D. Noble, SAPO-34 membranes for CO<sub>2</sub>/CH<sub>4</sub> separation., *Abstr Pap Am Chem S*, 227 (2004) U350-U350.
- [21] S.G. Li, J.L. Falconer, R.D. Noble, R. Krishna, Modeling permeation of CO<sub>2</sub>/CH<sub>4</sub>, CO<sub>2</sub>/N<sub>2</sub>, and N<sub>2</sub>/CH<sub>4</sub> mixtures across SAPO-34 membrane with the maxwell-stefan equations, *Industrial & Engineering Chemistry Research*, 46 (2007) 3904-3911.
- [22] X.Y. Luo, Y. Guo, F. Ding, H.Q. Zhao, G.K. Cui, H.R. Li, C.M. Wang, Significant Improvements in CO<sub>2</sub> Capture by Pyridine-Containing Anion-Functionalized Ionic Liquids through Multiple-Site Cooperative Interactions, *Angew Chem Int Edit*, 53 (2014) 7053-7057.
- [23] J. Cheng, L.Q. Hu, Y.N. Li, C.F. Ji, J.H. Zhou, K.F. Cen, Improving CO<sub>2</sub> permeability of ceramic hollow fibre-supported composite membranes by blending an ionic liquid in the Pebax/PEGDME selective layer, *Rsc Adv*, 6 (2016) 2055-2064.
- [24] W. Yuan, H. Chen, R. Chang, L. Li, Synthesis and characterization of high performance NaA

- zeolite-polyimide composite membranes on a ceramic hollow fiber by dip-coating deposition, Desalination, 273 (2011) 343-351.
- [25] W. Yave, A. Car, K.-V. Peinemann, Nanostructured membrane material designed for carbon dioxide separation, Journal of Membrane Science, 350 (2010) 124-129.
- [26] H.Z. Chen, Z. Thong, P. Li, T.-S. Chung, High performance composite hollow fiber membranes for CO<sub>2</sub>/H<sub>2</sub> and CO<sub>2</sub>/N<sub>2</sub> separation, International Journal of Hydrogen Energy, 39 (2014) 5043-5053.
- [27] Y.X. Wei, D.Z. Zhang, Y.L. He, L. Xu, Y. Yang, B.L. Su, Z.M. Liu, Catalytic performance of chloromethane transformation for light olefins production over SAPO-34 with different Si content, Catal Lett, 114 (2007) 30-35.
- [28] B. Mohammadkhani, M. Haghghi, P. Sadeghpour, Altering C<sub>2</sub>H<sub>4</sub>/C<sub>3</sub>H<sub>6</sub> yield in methanol to light olefins over HZSM-5, SAPO-34 and SAPO-34/HZSM-5 nanostructured catalysts: influence of Si/Al ratio and composite formation, Rsc Adv, 6 (2016) 25460-25471.
- [29] J. Cheng, Y.N. Li, L.Q. Hu, J.H. Zhou, K.F. Cen, CO<sub>2</sub> Adsorption Performance of Ionic Liquid [P-66614][2-Op] Loaded onto Molecular Sieve MCM-41 Compared to Pure Ionic Liquid in Biohythane/Pure CO<sub>2</sub> Atmospheres, Energ Fuel, 30 (2016) 3251-3256.
- [30] L.M. Robeson, The upper bound revisited, J Membrane Sci, 320 (2008) 390-400.
- [31] H.Z. Chen, Z.W. Thong, P. Li, T.S. Chung, High performance composite hollow fiber membranes for CO<sub>2</sub>/H-2 and CO<sub>2</sub>/N-2 separation, International Journal Of Hydrogen Energy, 39 (2014) 5043-5053.
- [32] C.H. Ma, W.J. Koros, High-performance ester-crosslinked hollow fiber membranes for natural gas separations, J Membrane Sci, 428 (2013) 251-259.
- [33] S.-H. Pak, Y.-W. Jeon, M.-S. Shin, H.C. Koh, Preparation of Cellulose Acetate Hollow-Fiber Membranes for CO<sub>2</sub>/CH<sub>4</sub>Separation, Environmental Engineering Science, (2015).
- [34] J.E. Ramírez-Morales, E. Tapia-Venegas, N. Nemestóthy, P. Bakonyi, K. Bélafi-Bakó, G. Ruiz-Filippi, Evaluation of two gas membrane modules for fermentative hydrogen separation, International Journal of Hydrogen Energy, 38 (2013) 14042-14052.
- [35] X.M. Jie, Y.M. Cao, B. Lin, Q. Yuan, Gas permeation performance of cellulose hollow fiber membranes made from the cellulose/N-methylmorpholine-N-oxide/H<sub>2</sub>O system, J Appl Polym Sci, 91 (2004) 1873-1880.
- [36] Z. Mao, X. Jie, Y. Cao, L. Wang, M. Li, Q. Yuan, Preparation of dual-layer cellulose/polysulfone hollow fiber membrane and its performance for isopropanol dehydration and CO<sub>2</sub> separation, Separation and Purification Technology, 77 (2011) 179-184.

## List of Figures and Tables:

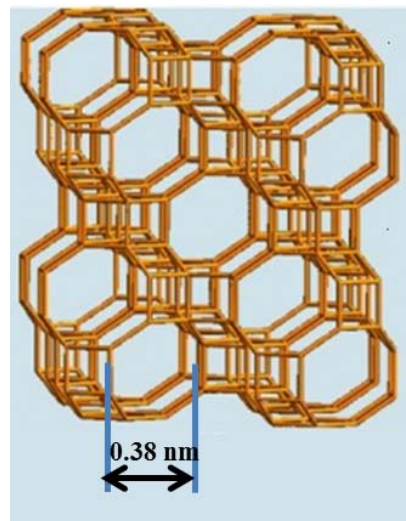
- Fig. 1 Structure (a) of SAPO 34 and illustration (b) of surface modification of SAPO 34 with NH<sub>2</sub> groups and Ionic Liquid (IL).
- Fig. 2 The schematic diagram of apparatus for measurement of gas permeance.
- Fig. 3 FTIR spectra of ionic liquid (IL), molecular sieve (SAPO 34), three composites of IL, and SAPO 34 with various weight ratios.
- Fig. 4 TGA profiles of ionic liquid (IL), molecular sieve (SAPO 34), three composites of IL, and SAPO 34 with various weight ratios.
- Fig. 5 Surface and cross-sectional SEM images of four mixed matrix membranes (MMMs) with molecular sieve (SAPO 34), three composites of IL, and SAPO 34 with various weight ratios.
- Fig. 6 AFM height images of surfaces of four mixed matrix membranes (MMMs) with molecular sieve (SAPO 34), three composites of IL, and SAPO 34 with various weight ratios.
- Fig. 7 AFM phase images of surfaces of four mixed matrix membranes (MMMs) with molecular sieve (SAPO 34), three composites of IL, and SAPO 34 with various weight ratios.
- Fig. 8 Effects of operating temperature on CO<sub>2</sub> permeances of four mixed matrix membranes (MMMs) with molecular sieve (SAPO 34), three composites of IL, and SAPO 34 with various weight ratios.
- Fig. 9 Effects of operating temperature on CO<sub>2</sub>/H<sub>2</sub> selectivity (a) and CO<sub>2</sub>/CH<sub>4</sub> selectivity (b) of four mixed matrix membranes (MMMs) with molecular sieve (SAPO 34), three composites of IL, and SAPO 34 with various weight ratios.
- Fig. 10 Comparison between this work and other studies on CO<sub>2</sub>/H<sub>2</sub> (a) and CO<sub>2</sub>/CH<sub>4</sub> (b) separation performance of mixed matrix membranes (MMMs).

Table 1 Roughness parameters of surfaces of four mixed matrix membranes (MMMs) with molecular sieve (SAPO 34), three composites of IL, and SAPO 34 with various weight ratios.

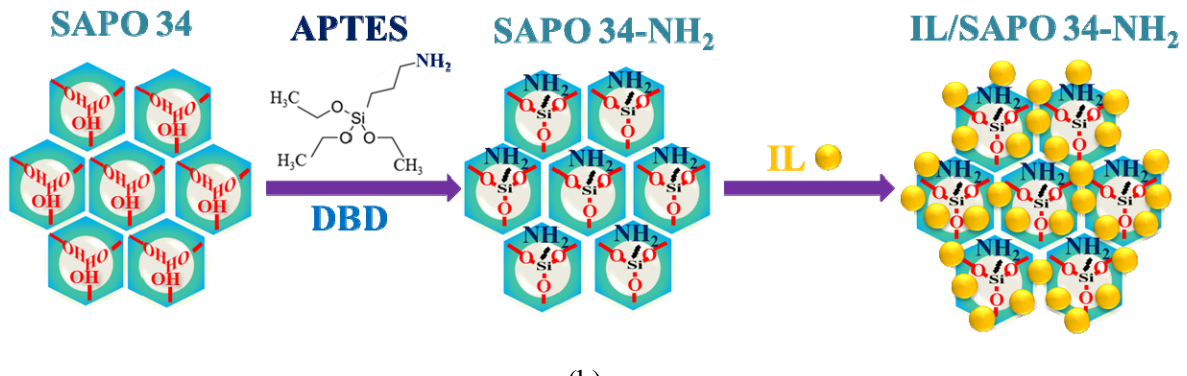
Table 2 CO<sub>2</sub>/H<sub>2</sub> and CO<sub>2</sub>/CH<sub>4</sub> separation performance of mixed matrix membranes

(MMMs) with molecular sieve (SAPO 34), three composites of IL, and SAPO 34 with various weight ratios.

Table 3 Comparison in CO<sub>2</sub> permeation and separation performance between ceramic hollow fiber-supported mixed matrix membranes (MMMs) in this study and hollow fiber CO<sub>2</sub>-philic polymer membranes reported in other studies.



(a)



(b)

Fig. 1 Structure (a) of SAPO 34 and illustration (b) of surface modification of SAPO 34 with NH<sub>2</sub> groups and Ionic Liquid (IL).

Notes: (1) SAPO 34-NH<sub>2</sub> stands for SAPO 34 modified with NH<sub>2</sub> groups.

(2) IL/SAPO 34-NH<sub>2</sub> stands for composite of IL and SAPO 34 modified with NH<sub>2</sub> groups.

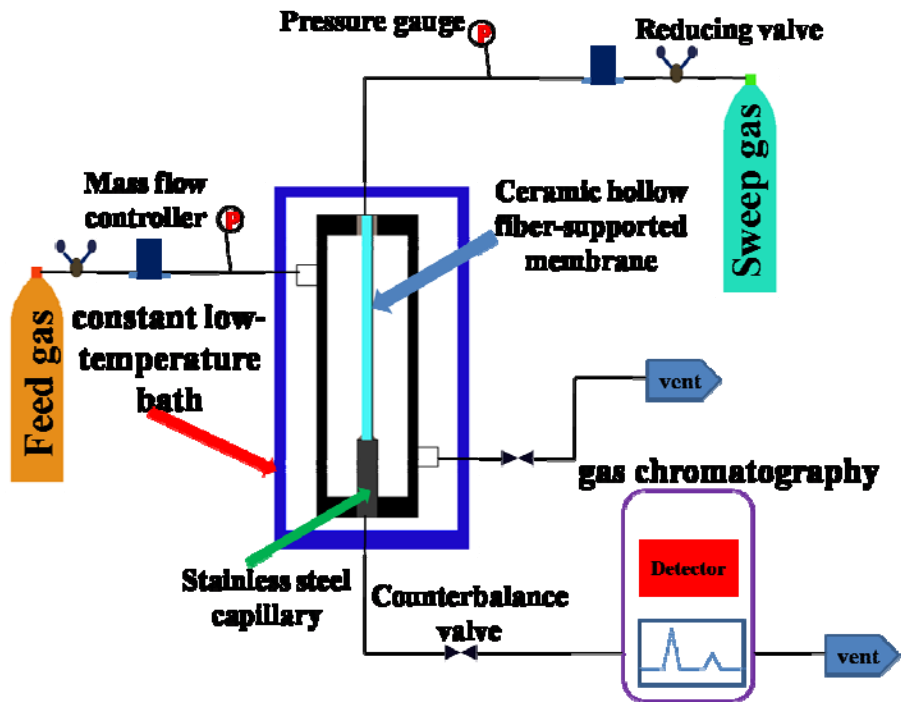


Fig. 2 The schematic diagram of apparatus for measurement of gas permeance.

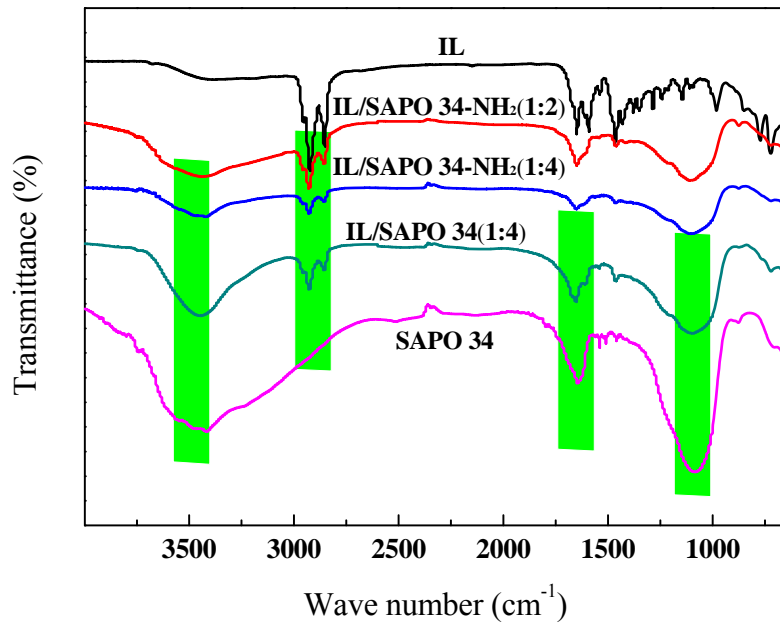


Fig. 3 FTIR spectra of ionic liquid (IL), molecular sieve (SAPO 34), three composites of IL, and SAPO 34 with various weight ratios.

Notes: (1) IL/SAPO 34 (1:4) stands for a composite of IL and SAPO 34 with a weight ratio of 1:4. (2) IL/SAPO 34-NH<sub>2</sub> (1:4) stands for a composite of IL and SAPO 34 (modified with NH<sub>2</sub> group) with a weight ratio of 1:4. (3) IL/SAPO 34-NH<sub>2</sub> (1:2) stands for a composite of IL and SAPO 34 (modified with NH<sub>2</sub> group) with a weight ratio of 1:2.

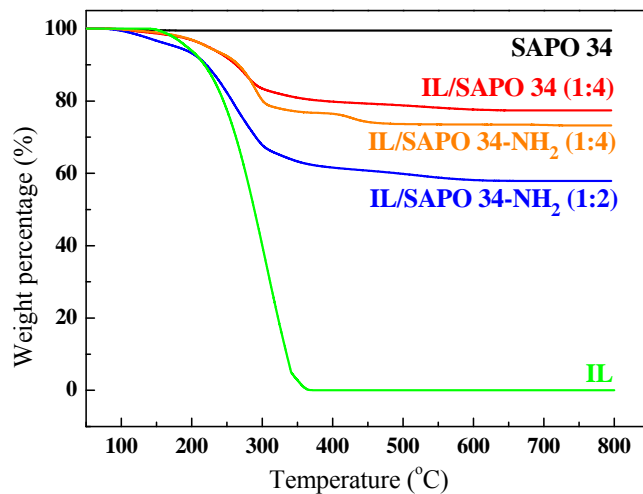


Fig. 4 TGA profiles of ionic liquid (IL), molecular sieve (SAPO 34), three composites of IL, and SAPO 34 with various weight ratios.

Notes: (1) IL/SAPO 34 (1:4) stands for a composite of IL and SAPO 34 with a weight ratio of 1:4. (2) IL/SAPO 34-NH<sub>2</sub> (1:4) stands for a composite of IL and SAPO 34 (modified with NH<sub>2</sub> group) with a weight ratio of 1:4. (3) IL/SAPO 34-NH<sub>2</sub> (1:2) stands for a composite of IL and SAPO 34 (modified with NH<sub>2</sub> group) with a weight ratio of 1:2.

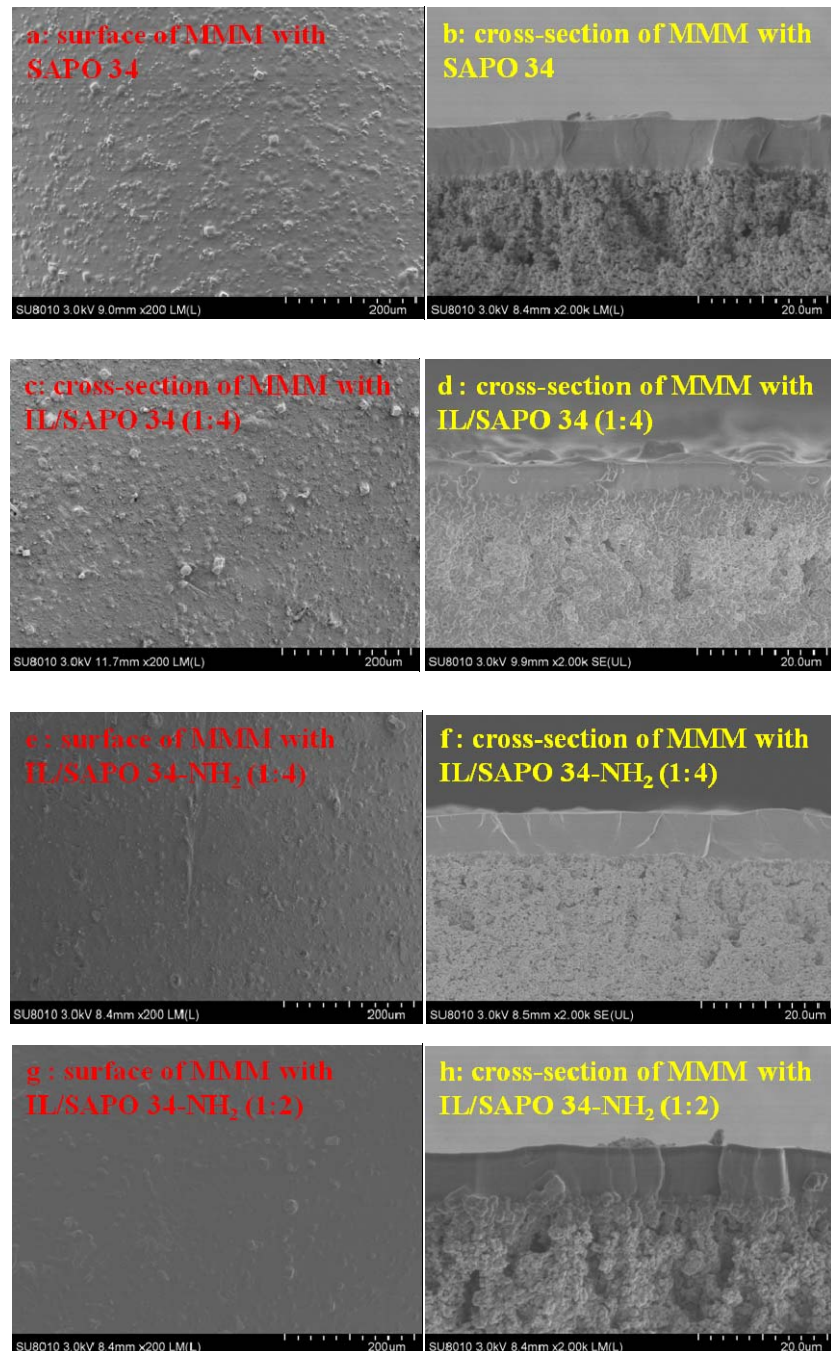


Fig. 5 Surface and cross-sectional SEM images of four mixed matrix membranes (MMMs) with molecular sieve (SAPO 34), three composites of IL, and SAPO 34 with various weight ratios.

Notes: (1) IL/SAPO 34 (1:4) stands for a composite of IL and SAPO 34 with a weight ratio of 1:4. (2) IL/SAPO 34-NH<sub>2</sub> (1:4) stands for a composite of IL and SAPO 34 (modified with NH<sub>2</sub> group) with a weight ratio of 1:4. (3) IL/SAPO 34-NH<sub>2</sub> (1:2) stands for a composite of IL and SAPO 34 (modified with NH<sub>2</sub> group) with a weight ratio of 1:2.

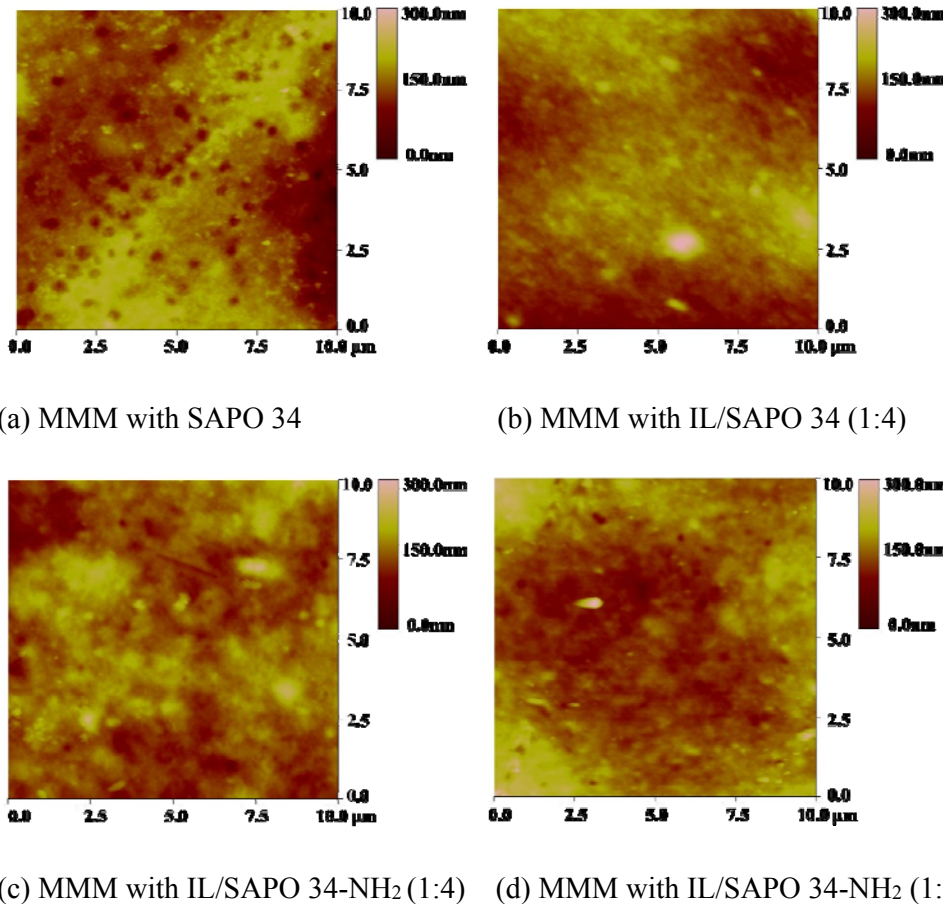


Fig. 6 AFM height images of surfaces of four mixed matrix membranes (MMMs) with molecular sieve (SAPO 34), three composites of IL, and SAPO 34 with various weight ratios.

Notes: (1) IL/SAPO 34 (1:4) stands for a composite of IL and SAPO 34 with a weight ratio of 1:4. (2) IL/SAPO 34-NH<sub>2</sub> (1:4) stands for a composite of IL and SAPO 34 (modified with NH<sub>2</sub> group) with a weight ratio of 1:4. (3) IL/SAPO 34-NH<sub>2</sub> (1:2) stands for a composite of IL and SAPO 34 (modified with NH<sub>2</sub> group) with a weight ratio of 1:2.

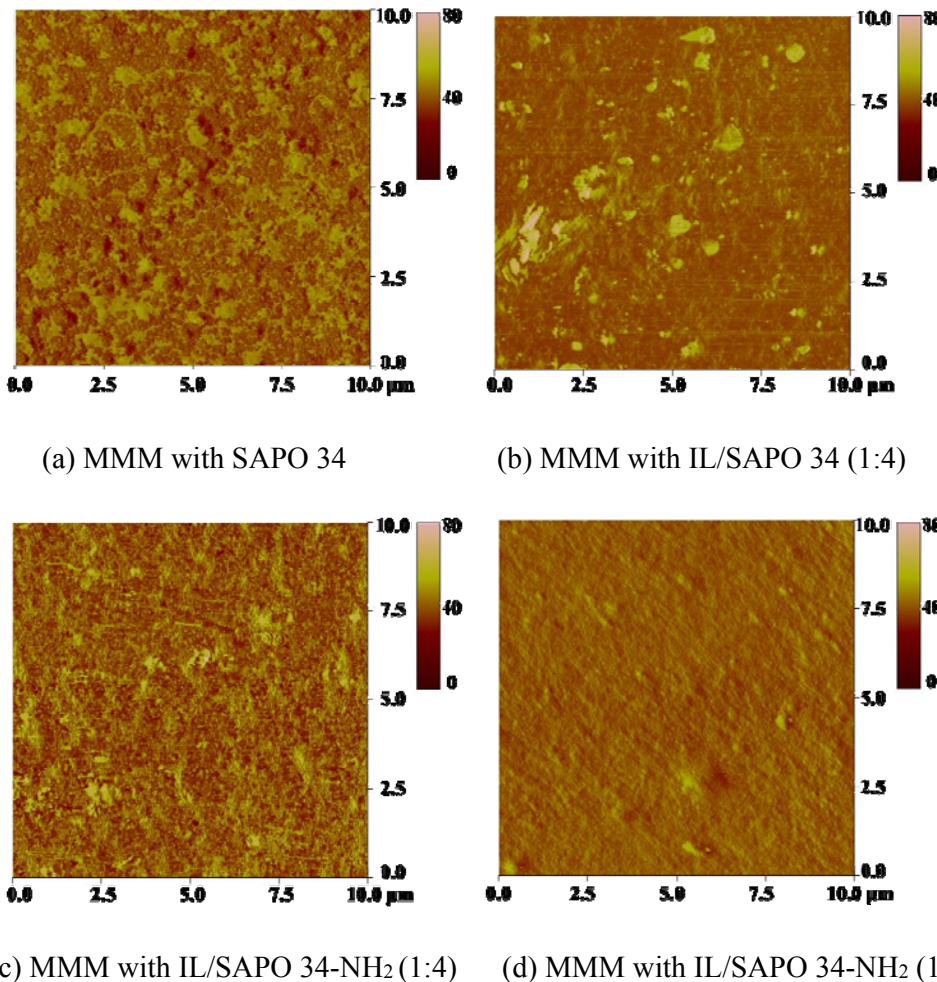


Fig. 7 AFM phase images of surfaces of four mixed matrix membranes (MMMs) with molecular sieve (SAPO 34), three composites of IL, and SAPO 34 with various weight ratios.

Notes: (1) IL/SAPO 34 (1:4) stands for a composite of IL and SAPO 34 with a weight ratio of 1:4. (2) IL/SAPO 34-NH<sub>2</sub> (1:4) stands for a composite of IL and SAPO 34 (modified with NH<sub>2</sub> group) with a weight ratio of 1:4. (3) IL/SAPO 34-NH<sub>2</sub> (1:2) stands for a composite of IL and SAPO 34 (modified with NH<sub>2</sub> group) with a weight ratio of 1:2.

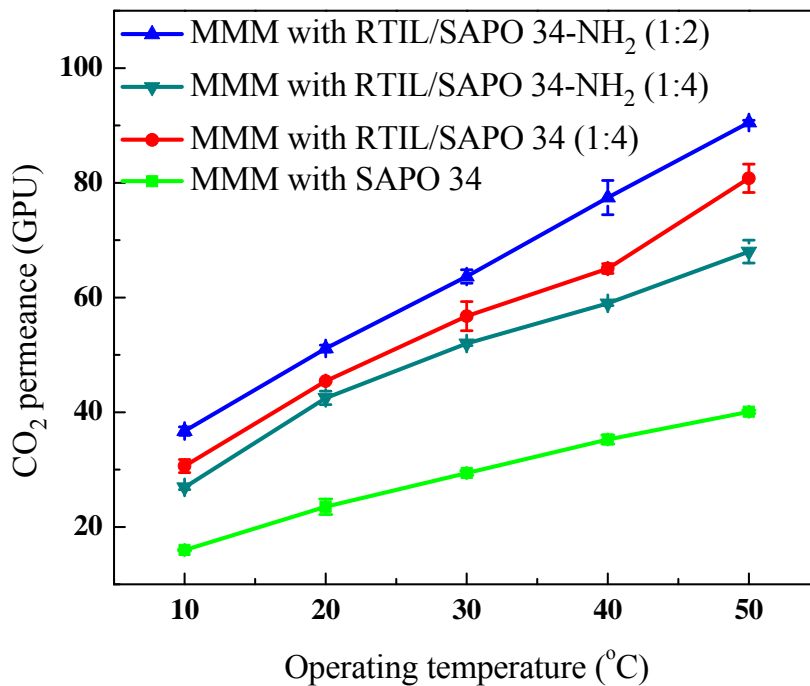


Fig. 8 Effects of operating temperature on CO<sub>2</sub> permeances of four mixed matrix membranes (MMMs) with molecular sieve (SAPO 34), three composites of IL, and SAPO 34 with various weight ratios.

Notes: (1) IL/SAPO 34 (1:4) stands for a composite of IL and SAPO 34 with a weight ratio of 1:4. (2) IL/SAPO 34-NH<sub>2</sub> (1:4) stands for a composite of IL and SAPO 34 (modified with NH<sub>2</sub> group) with a weight ratio of 1:4. (3) IL/SAPO 34-NH<sub>2</sub> (1:2) stands for a composite of IL and SAPO 34 (modified with NH<sub>2</sub> group) with a weight ratio of 1:2. Fig. 7 Effects of operating temperature on CO<sub>2</sub> permeation rates of four mixed matrix membranes (MMMs) with molecular sieve (SAPO 34), three composites of IL, and SAPO 34 with various weight ratios.

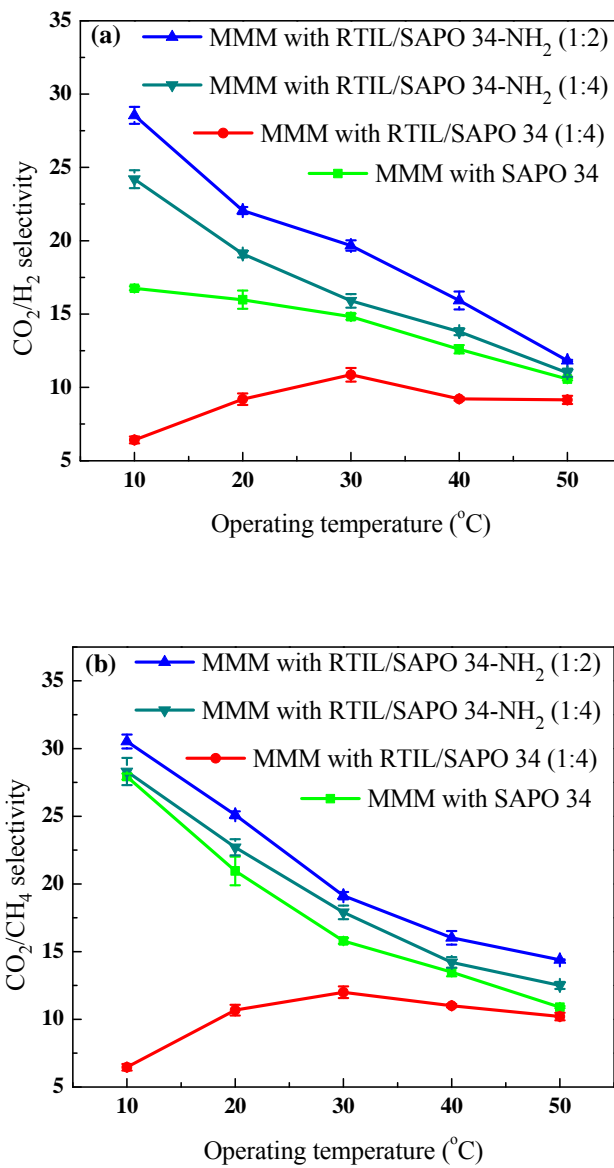


Fig. 9 Effects of operating temperature on CO<sub>2</sub>/H<sub>2</sub> selectivity (a) and CO<sub>2</sub>/CH<sub>4</sub> selectivity (b) of four mixed matrix membranes (MMMs) with molecular sieve (SAPO 34), three composites of IL, and SAPO 34 with various weight ratios.

Notes: (1) IL/SAPO 34 (1:4) stands for a composite of IL and SAPO 34 with a weight ratio of 1:4. (2) IL/SAPO 34-NH<sub>2</sub> (1:4) stands for a composite of IL and SAPO 34 (modified with NH<sub>2</sub> group) with a weight ratio of 1:4. (3) IL/SAPO 34-NH<sub>2</sub> (1:2) stands for a composite of IL and SAPO 34 (modified with NH<sub>2</sub> group) with a weight ratio of 1:2.

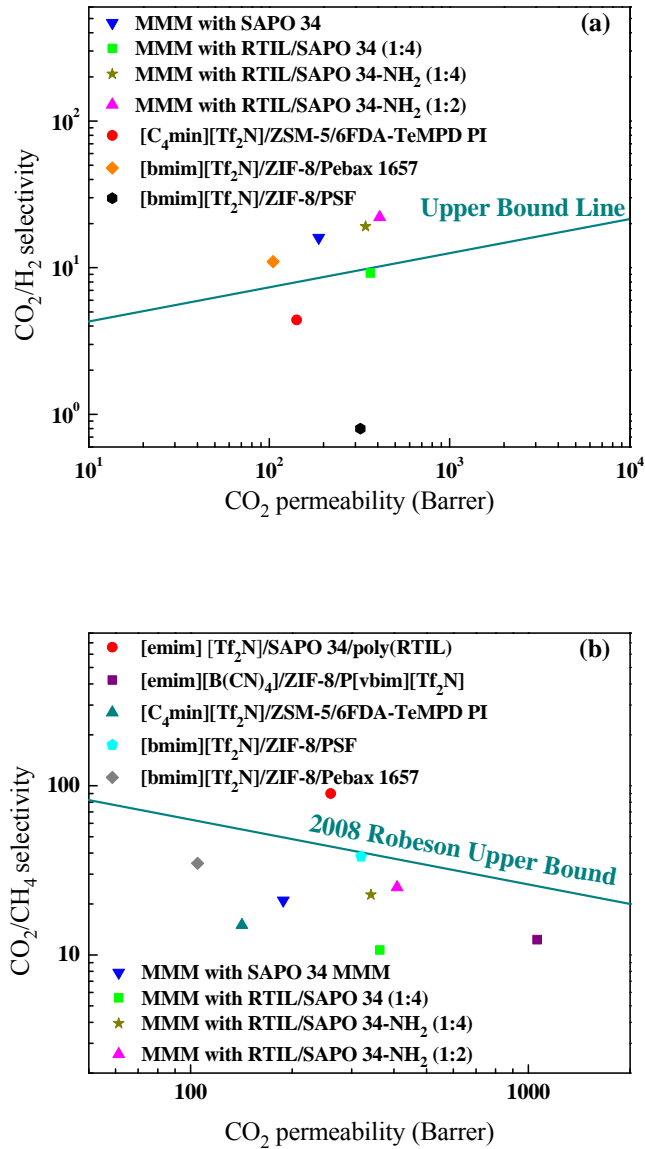


Fig. 10 Comparison between this work and other studies on CO<sub>2</sub>/H<sub>2</sub> (a) and CO<sub>2</sub>/CH<sub>4</sub> (b) separation performance of mixed matrix membranes (MMMs).

Notes: (1) IL/SAPO 34 (1:4) stands for a composite of IL and SAPO 34 with a weight ratio of 1:4. (2) IL/SAPO 34-NH<sub>2</sub> (1:4) stands for a composite of IL and SAPO 34 (modified with NH<sub>2</sub> group) with a weight ratio of 1:4. (3) IL/SAPO 34-NH<sub>2</sub> (1:2) stands for a composite of IL and SAPO 34 (modified with NH<sub>2</sub> group) with a weight ratio of 1:2; (4) operating temperature for those values in this study is 20 °C.

Table 1 Roughness parameters of surfaces of four mixed matrix membranes (MMMs) with molecular sieve (SAPO 34), three composites of IL, and SAPO 34 with various weight ratios.

Roughness parameters	$R_{ms}$ (nm)	$R_a$ (nm)
MMM with SAPO 34	37.5	30.1
MMM with IL/SAPO 34 (1:4)	30.3	24.3
MMM with IL/SAPO 34-NH <sub>2</sub> (1:4)	27.6	22.2
MMM with IL/SAPO 34-NH <sub>2</sub> (1:2)	27.3	21.5

Notes: (1) IL/SAPO 34 (1:4) stands for a composite of IL and SAPO 34 with a weight ratio of 1:4. (2) IL/SAPO 34-NH<sub>2</sub> (1:4) stands for a composite of IL and SAPO 34 (modified with NH<sub>2</sub> group) with a weight ratio of 1:4. (3) IL/SAPO 34-NH<sub>2</sub> (1:2) stands for a composite of IL and SAPO 34 (modified with NH<sub>2</sub> group) with a weight ratio of 1:2. (4)  $R_{ms}$  and  $R_a$  stand for the root-mean-square deviation of height and average deviation of height based on AFM analysis, respectively.)

Table 2 CO<sub>2</sub>/H<sub>2</sub> and CO<sub>2</sub>/CH<sub>4</sub> separation performance of mixed matrix membranes (MMMs) with molecular sieve (SAPO 34), three composites of IL and SAPO 34 with various weight ratios.

<b>Membranes</b>	<b>P(CO<sub>2</sub>) (Barrers)</b>	<b>P(H<sub>2</sub>) (Barrers)</b>	<b>P(CH<sub>4</sub>) (Barrers)</b>	<b>CO<sub>2</sub>/H<sub>2</sub> selectivity</b>	<b>CO<sub>2</sub>/CH<sub>4</sub> selectivity</b>
Pebax/PEGMDE <sup>a</sup>	229.6	12.8	11.9	18.0	19.3
Pebax/PEGMDE/IL <sup>a</sup>	307.6	17.7	15.7	17.4	19.6
MMM with SAPO 34	188.2	11.8	8.9	16.0	21.0
MMM with IL/SAPO 34 (1:4)	363.4	39.5	41.8	9.2	10.7
MMM with IL/SAPO 34-NH <sub>2</sub> (1:4)	342.2	17.9	18.8	19.1	22.7
MMM with IL/SAPO 34-NH <sub>2</sub> (1:2)	408.9	18.5	20.3	22.1	25.1

Note: <sup>a</sup> reported in previous work [23].

Table 3 Comparison in CO<sub>2</sub> permeation and separation performance between ceramic hollow fiber-supported mixed matrix membranes (MMMs) in this study and hollow fiber CO<sub>2</sub>-philic polymer membranes reported in other studies.

Membranes	Configuration	Testing temperature (°C) / pressure (bar)	CO <sub>2</sub> permeation rate (GPU)	CO <sub>2</sub> /H <sub>2</sub> selectivity	CO <sub>2</sub> /CH <sub>4</sub> selectivity	References
Ester-crosslinkable	Single layer	35 / ~13.8	117	-	37	[32]
PDMS-Cellulose Acetate	Single layer	~25 / 3	12.9	-	43.8	[33]
cellulose	Single layer	25 / 5	0.6	15.8	30.0	[35]
PDMS	Single layer	23 / 1.2	~59.7	6.1	-	[34]
cellulose/PSF	Dual layer	35 / 3	3.1	17.1	38.0	[36]
Pebax-PEGDME/ceramic	Dual layer	20 / 1	29.7	18.0	19.1	[23]
Pebax-PEGDME-IL/ceramic	Dual layer	20 / 1	41.1	17.4	19.6	
MMM with SAPO 34	Dual layer	20 / 1	23.5	16.0	21.0	This study
MMM with IL/SAPO 34 (1:4)	Dual layer	20 / 1	45.4	9.2	10.7	
MMM with IL/SAPO 34-NH <sub>2</sub> (1:4)	Dual layer	20 / 1	42.5	19.1	22.7	
MMM with IL/SAPO 34-NH <sub>2</sub> (1:2)	Dual layer	20 / 1	51.1	22.1	25.1	